ACS Sustainable Resource Management

pubs.acs.org/acssrm

Letter

COFfee: A Coffee Waste@Anthraquinone COF Nanocomposite as a Photocatalyst for Green Hydrogen Production

Astha Singh, Swadhin K. Jena, Prem F. Siril, and Moritz F. Kühnel*

Cite This: *ACS Sustainable Resour. Manage.* 2026, 3, 45−51

Read Online

ACCESS | Metrics & More | Article Recommendations | Supporting Information

ABSTRACT: Sustainability is pivotal for the growth, development, and survival of future generations, necessitating a shift to renewable energy sources and sustainable materials. The development of waste-derived, visible-light-active, nontoxic photocatalysts for water splitting is a promising approach in this direction. We report the one-pot synthesis of a novel waste coffee (WC)-based covalent organic framework (COF) nanocomposite, WC@DqTp, via a vortex-assisted solvothermal method. Integrating an anthraquinone-based COF (DqTp) with WC enhances its photocatalytic performance through improved charge separation. The photocatalytic activity of WC@DqTp for hydrogen evolution from water using platinum as a co-catalyst without an added sacrificial agent (36.1 μmol g^{-1} h^{-1}) was almost two times higher than that of bare COF DqTp (21.2 μmol g^{-1} h^{-1}). XPS, photoelectrochemistry, and PL lifetime measurements demonstrated that the superior efficiency of the nanocomposite is likely due to the formation of a Z-scheme heterojunction between WC and DqTp. This work highlights the potential of sustainable materials as efficient photocatalysts for green hydrogen generation.

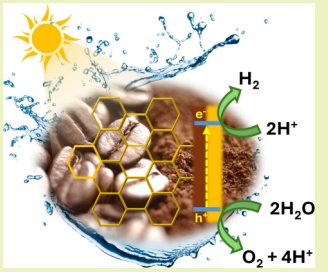

INTRODUCTION

Sustainability is key for the growth, development, and survival of future generations. With the continuous depletion of fossil resources, the urge to use renewable alternatives is increasing day by day. Additionally, burning fossil fuels not only damages the ecosystem but also affects human health. To circumvent the repercussions of traditional fuels, researchers have focused on developing a means of generating green fuels from renewable sources of energy. The production of green hydrogen from water splitting and waste reforming are particularly promising.[1] However, major challenges in this approach include the large-scale production, storage, and transportation of green hydrogen[2] as well as the industry-scale testing of these technologies.[3] Moreover, electrochemical water splitting requires large amounts of energy that is not available at a low price, nor is its distribution compatible with the existing grid infrastructure. Technoeconomic analyses have highlighted that simple suspension photocatalysis may allow low-cost H_2 production without complex setup and disproportionate investment costs.[4,5]

Photocatalysis for the production of green hydrogen from water requires energy to drive the reaction and a catalyst for improving the reaction kinetics. The direct use of sunlight represents the most sustainable and renewable energy source due to its high abundance,[6] with visible light constituting 47% of the solar spectrum. It is therefore imperative to develop visible-light-active catalysts, ideally based on nontoxic and affordable materials. While metal-based photocatalysts are highly efficient, they often suffer from high costs and metal leaching, reducing the economic viability of H_2 production.[7−9]

Conjugated porous organic polymers (CPOPs), a subclass of covalent organic frameworks (COFs), are promising metal-free photocatalysts, fueled by the discovery of COF-5 in 2005.[10] However, in single-component photocatalysts, rapid electron−hole recombination limits the availability of charge carriers for photocatalytic reactions.[7] The development of photocatalysts based on a Z-scheme heterojunction not only improves the charge separation but also spatially separates the oxidation and reduction half-reactions.[8,11,12] Using waste as a feedstock to facilitate light-driven fuel generation has achieved growing attention, e.g., photoreforming of plastics or wastewater treatment.[13−16] Interestingly, synthesizing the photocatalyst itself from waste is much less explored with only a few examples, including waste-derived metal−organic frameworks,[17] carbon-based 2D materials,[18−20] quantum dots,[21] porous carbon,[22] and metal oxides/sulfides and their nanocomposites.[23] However, waste-derived CPOP composites have not yet been reported.

According to the International Coffee Organization, coffee is one of the most consumed drinks worldwide, with annual consumption rising by over 10 million tons since 2018.[24] The major waste product of secondary coffee processing is waste coffee grounds (WC), which may reach up to 15 million tons per year globally.[25] A lack of energy-efficient processing methods for this waste leads to disposal in landfills with negative impacts on air and soil quality.[26,27] Therefore, a direct,

Received: September 8, 2025
Revised: November 21, 2025
Accepted: November 24, 2025
Published: December 22, 2025

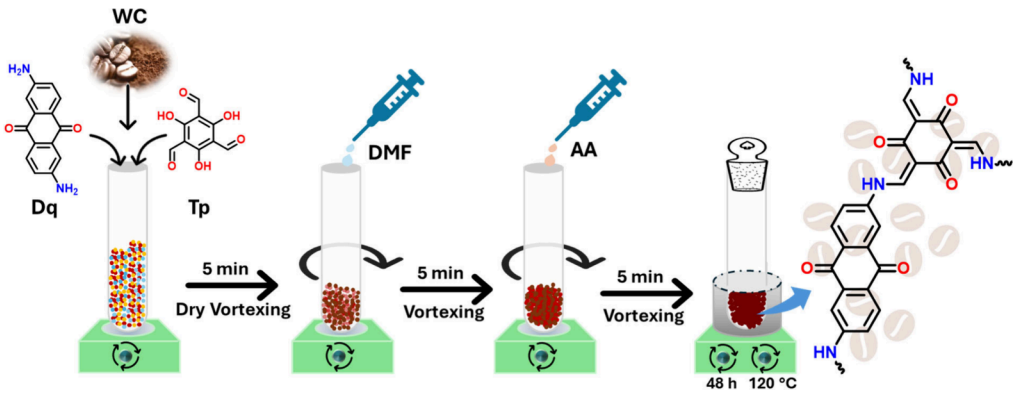

Figure 1. Schematic representation of the one-pot synthesis procedure for the WC@DqTp nanocomposite.

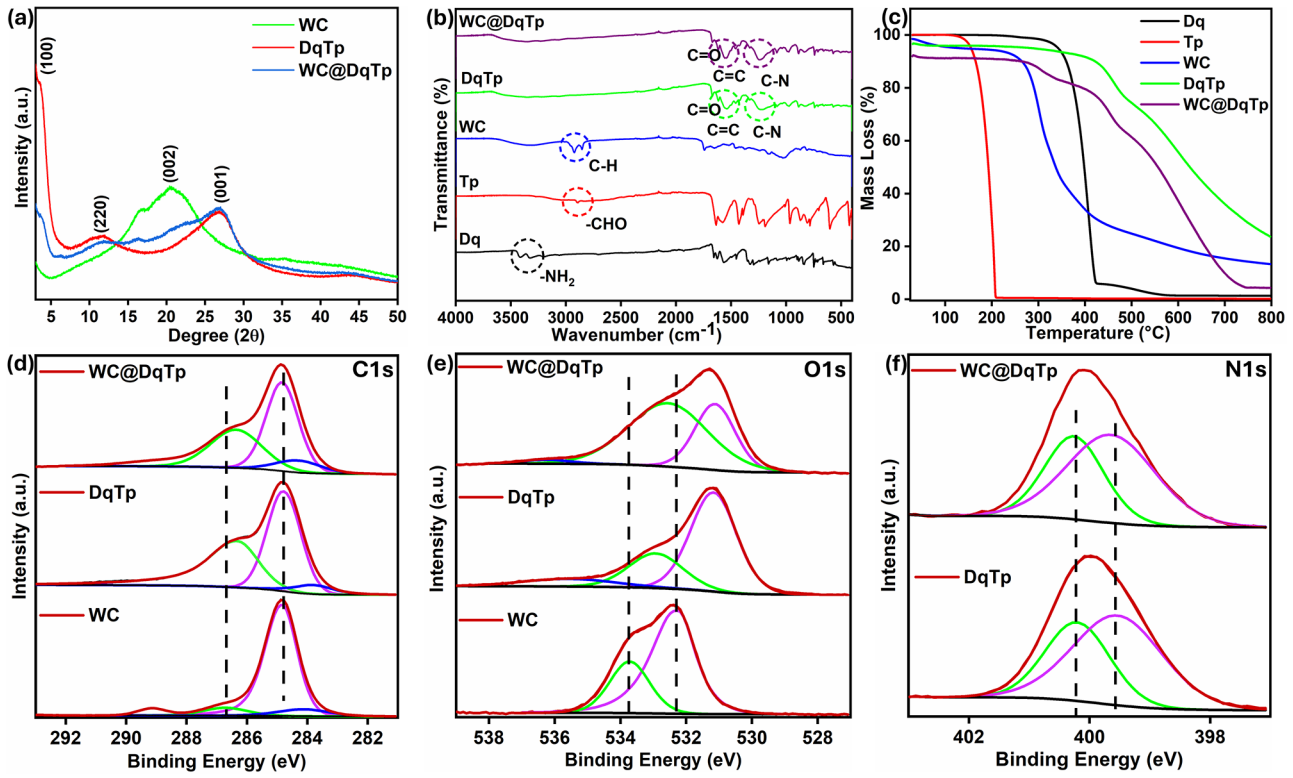

Figure 2. Physicochemical characterization of WC, DqTp, and WC@DqTp. (a) pXRD patterns, (b) FTIR spectra, and (c) TGA curves. XPS spectra of WC, DqTp, and WC@DqTp in the (d) C 1s, (e) O 1s, and (f) N 1s regions.

purposeful utilization of WC without energy-intensive processing is highly desirable to mitigate pollution.

Herein, we demonstrate that the WC can be used to synthesize a COF nanocomposite with favorable photocatalytic activity for H_2 generation. We have used a one-pot solvothermal method to prepare a nanocomposite, WC@DqTp, from WC and an anthraquinone-based COF that was fully characterized. Furthermore, we show that it can be used as a photocatalyst for the generation of H_2 from water using a Pt co-catalyst without an added sacrificial agent. A comparison of its photocatalytic activity with that of bare WC and DqTp corroborated by spectroscopic evidence proves that improved charge separation due to heterojunction formation is an effective strategy to enhance photocatalytic activity.

RESULTS AND DISCUSSIONS

The one-pot solvothermal synthesis of a nanocomposite from waste coffee (WC) and the anthraquinone-based COF DqTp was achieved through the formation of β-ketoenamine linkages upon acetic acid (AA)-catalyzed polycondensation of the diamine 2,6-diaminoanthraquinone (Dq) with the trialdehyde 1,3,5-triformylphloroglucinol (Tp)[28] (the procedure is shown schematically in Figure 1).

Evidence for the successful nanocomposite synthesis was sought from powder XRD (Figure 2a), which compares the XRD pattern of WC@DqTp to those of WC and DqTp. As expected, all materials show broad reflections consistent with a low crystallinity. A peak at $2\theta = 3.61°$ corresponds to the characteristic (100) plane of the DqTp COF. Additional small peaks at $2\theta \approx 11.7°$ and 26.9° can be assigned to the (220) and (001) planes, respectively.[29] The presence of a broad (001) reflection due to interlayer $\pi-\pi$ stacking indicates the layered

https://doi.org/10.1021/acssusresmgt.5c00454
ACS Sustainable Resour. Manage. 2026, 3, 45−51

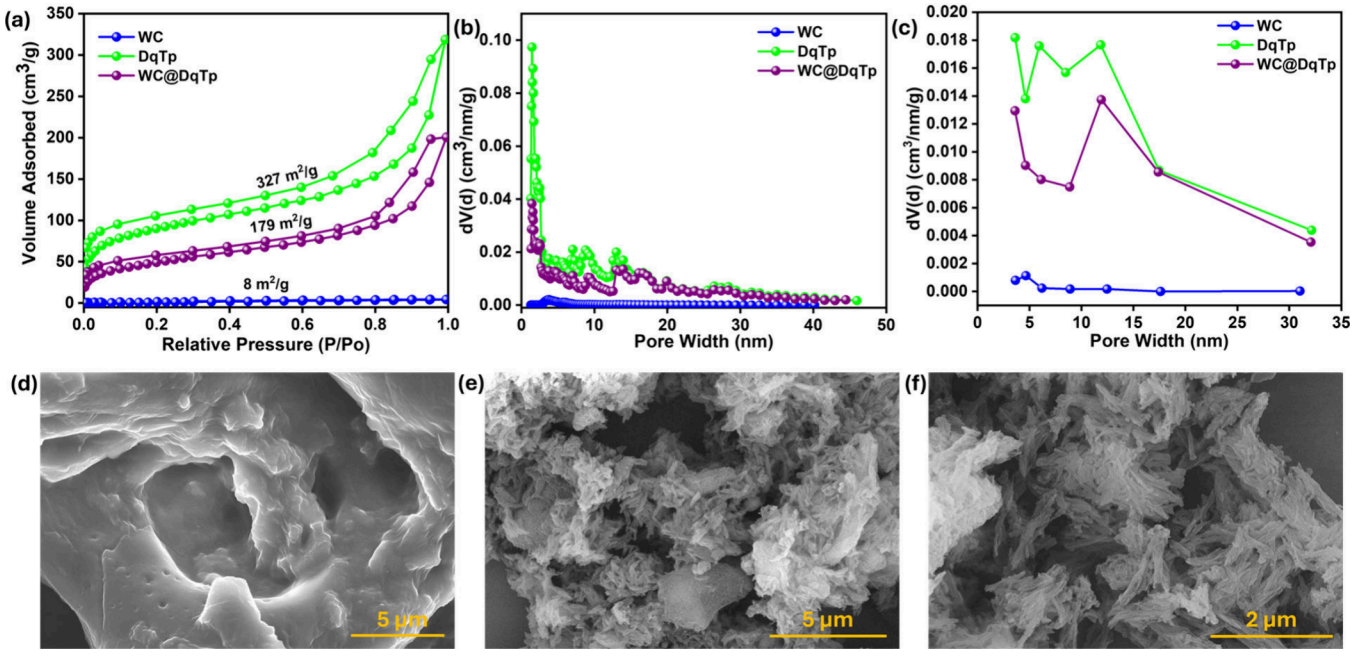

Figure 3. Morphological characterization for WC, DqTp, and WC@DqTp. (a) N_2 adsorption−desorption isotherms, (b) NLDFT micropore size distributions, and (c) BJH mesopore size distributions. FESEM images of (d) WC, (e) DqTp, and (f) WC@DqTp.

COF structure with an interlayer distance calculated at ∼3.2 Å in the DqTp COF. Upon introduction of WC into the DqTp framework, the intensity of the (100) reflection is reduced, confirming the amalgamation of WC and DqTp.[28] Furthermore, a new reflection is observed at 16.16° in the XRD pattern of WC@DqTp that is well matched with the peak of bare WC, confirming the introduction of WC into the DqTp framework. A broad peak at 20.6° in the WC XRD pattern corresponds to the (002) plane, attributable to a cellulosic structure.[30,31]

Functional group analysis using vibrational spectroscopy further confirmed the composite formation. Figure 2b shows the FTIR spectra of all materials and their respective reactants for comparison. The presence of peaks at 1608 and 1223 cm^{-1} in DqTp indicates C═O and C−N functional groups, consistent with the formation of a β-ketoenamine linkage.[32] At the same time, the −CHO (2888 cm^{-1}) and $-NH_2$ (3402 cm^{-1}) functional groups of the respective monomers (Tp and Dq) are no longer detectable in the DqTp COF. Additionally, after nanocomposite formation, the C═O and C−N peaks in WC@DqTp are shifted to higher wavenumbers compared to DqTp, confirming nanocomposite formation (Figure S1a).[33] This shift may be due to changes in the chemical environment of these functional groups upon the introduction of WC into the DqTp matrix.[34]

Nanocomposite formation was further studied by using TGA (Figure 2c). DqTp shows an enhanced thermal stability up to 400 °C compared to its monomers, whereas the stability of the nanocomposite WC@DqTp was reduced with three distinct stages of decomposition.[35] The first step at around 300 °C matches the decomposition of pure WC and can therefore be attributed to the degradation of its WC constituent. The second decomposition at around 400 °C matches the decomposition of pure DqTp, attributed to COF degradation. The final decomposition near 500 °C, similarly observed in pure DqTp, is likely due to the breaking of its carbon skeleton, confirming that the nanocomposite is composed of both WC and DqTp.

The chemical interaction and functionalities of the synthesized materials were further investigated using XPS (Figures S2−S4).[36] The C 1s spectrum of WC@DqTp shows peaks at 284.8 (C═C) and 286.6 eV (C−O), slightly shifted to higher and lower binding energies, respectively, in comparison with the respective peaks in DqTp and WC (Figure 2d). The peak at 289.1 eV in WC, assigned to O—C═O, is no longer visible in WC@DqTp. In contrast, the O 1s peak of WC@DqTp is shifted to a lower binding energy in comparison to that of bare DqTp, suggesting a transfer of electrons from WC to DqTp (Figure 2e).[36] However, there is no difference in the N 1s binding energy (Figure 2f), confirming that the shift is evident only for the elements of WC that directly interact with DqTp. This evidence proves a chemical interaction between WC and DqTp, consistent with the formation of a nanocomposite.

Surface analysis using N_2 adsorption−desorption isotherms at 77 K shows a combination of both micropores and mesopores, indicated by a H4-type hysteresis (Figure 3a) in the Type-IV(a) isotherm.[37,38] Multipoint BET analysis (p/p_0 0.03−0.25) gave a surface area of 327 $m^2\ g^{-1}$ for DqTp, whereas WC is essentially nonporous with a surface area of only 8 $m^2\ g^{-1}$. In the nanocomposite WC@DqTp, the surface area was slightly reduced to 179 $m^2\ g^{-1}$ due to the insertion of WC into the DqTp matrix;[33] however, the porous structure remains intact. The Langmuir surface areas of WC, DqTp, and WC@DqTp were determined to be 50, 416, and 262 $m^2\ g^{-1}$, respectively. Pore size distribution analysis using NLDFT shows that both DqTp and WC@DqTp are microporous with a maximum at a pore size of 1.5 nm. However, WC@DqTp has a lower abundance of micropores compared to DqTp that we attribute to the inclusion of WC into the DqTp structure (Figure 3b).[28,33] Moreover, BJH analysis reveals that both materials also have mesopores in their structures (Figure 3c). The $v-t$ plot analysis gave a microporous surface area of 145

https://doi.org/10.1021/acssusresmgt.5c00454
ACS Sustainable Resour. Manage. 2026, 3, 45−51

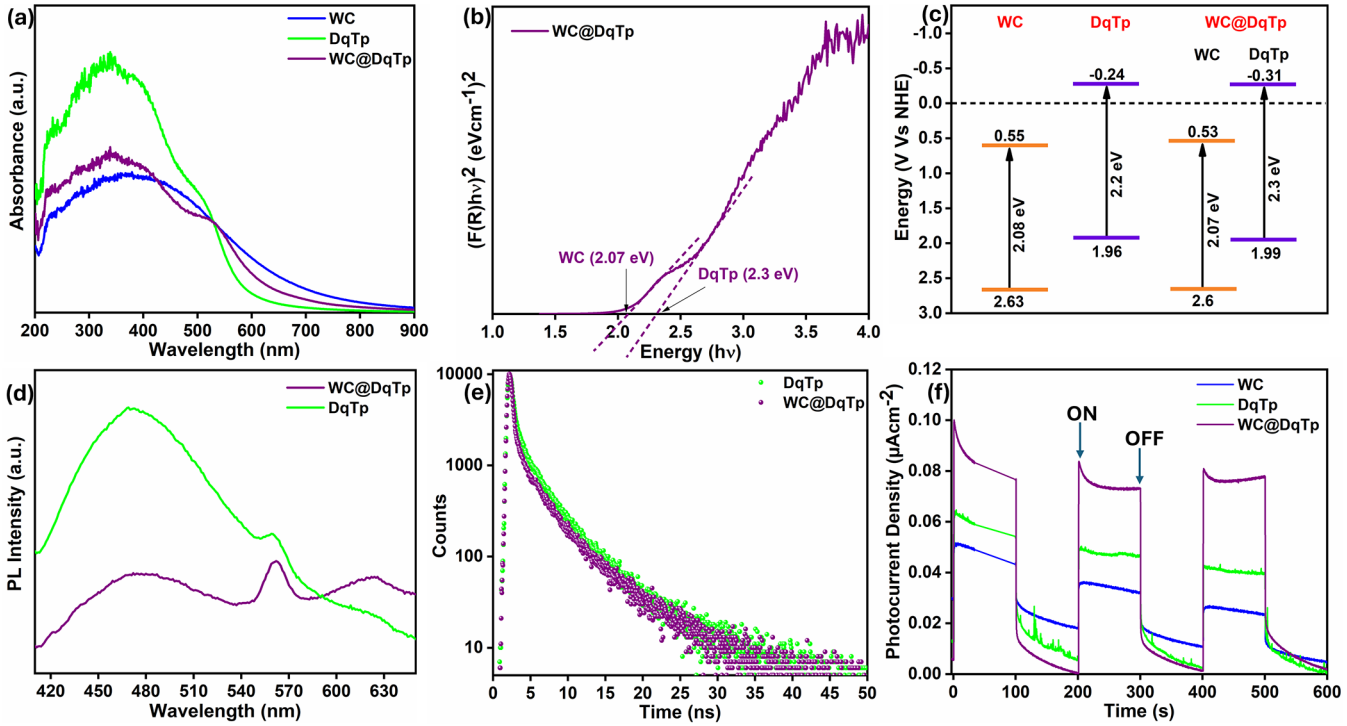

Figure 4. Optical and electronic properties of WC, DqTp, and WC@DqTp. (a) UV-DRS spectra, (b) Tauc plots, (c) band diagram, (d) steady-state photoluminescence spectra, (e) photoluminescence lifetime, and (f) photocurrent measurements under chopped illumination.

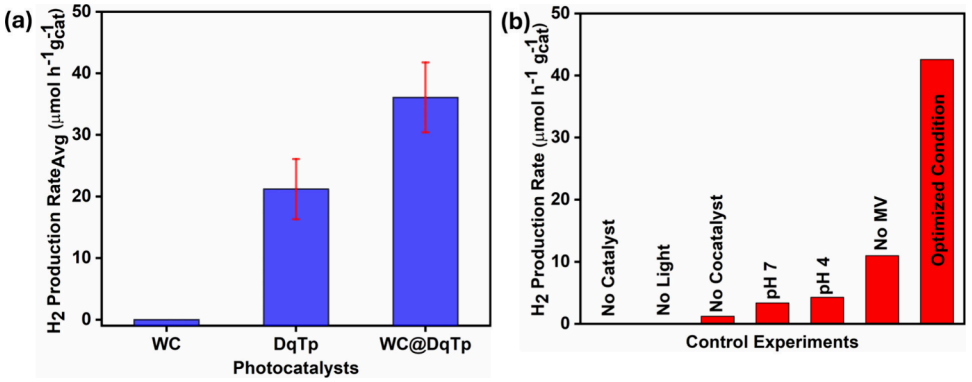

Figure 5. Photocatalytic H_2 evolution using WC@DqTp. (a) H_2 evolution rates using WC, DqTp, and WC@DqTp. (b) Control experiments for photocatalytic H_2 evolution using WC@DqTp (conditions: 1 mg of photocatalyst, 2 mL of H_2O (pH 2), 1 wt % Pt, 2 mM MV, 10 h of AM 1.5G irradiation, 1 sun).

$m^2\ g^{-1}$ and an external surface area of 182 $m^2\ g^{-1}$ for DqTp, whereas the microporous and external surface areas of WC@DqTp were reduced to 47 and 132 $m^2\ g^{-1}$, respectively.

FESEM shows that while WC exhibits a random bulky morphology consistent with its aforementioned nonporosity, DqTp and WC@DqTp feature a nanofibrous structure matching their high surface areas (Figure 3d–f), which in turn supports efficient mass transport and more active sites, making them suitable for photocatalytic applications.

UV-DRS spectra of DqTp and WC@DqTp show a broad absorbance across the UV, visible, and NIR range with a shoulder at ~500 nm (Figure 4a), due to $\pi-\pi^*$ and $n-\pi^*$ transitions in the C=C and C=O functional groups, respectively. The absorption maxima of WC@DqTp are slightly shifted toward longer wavelengths in comparison to those of bare DqTp. This may be due to extended conjugation after nanocomposite formation, confirming enhanced light harvesting of the WC@DqTp nanocomposite.[39] The Tauc plot analysis for WC@DqTp showed a direct band gap of 2.3 eV, closely resembling the band gap of bare DqTp (2.2 eV), as well as another transition at 2.07 eV (Figure 4b), which matches the optical band gap of bare WC (2.08 eV; Figure S1b).

The valence band maxima were determined directly by using ultraviolet photoelectron spectroscopy (UPS). The valence band maxima were used to determine the conduction band minima from the optical band gap values obtained from the Tauc plot (see Table S1 for details). Figure 4c shows the resulting band structure of WC@DqTp with a Z-scheme heterojunction alignment between the WC and COF components, expected to result in favorable photocatalytic properties due to reduced charge recombination.[40]

Steady-state photoluminescence (PL) spectroscopy of DqTp and WC@DqTp at an excitation wavelength of 350 nm (Figure 4d) showed a broad emission range with a maximum

https://doi.org/10.1021/acssusresmgt.5c00454
ACS Sustainable Resour. Manage. 2026, 3, 45–51

at 480 nm,[41] which was noticeably reduced in WC@DqTp in comparison to DqTp, suggesting reduced charge recombination and better charge transportation.[42] Time-resolved photoluminescence (TRPL) recorded by using 375 nm excitation (Figure 4e) showed only a marginal effect of the composite formation on the charge carrier lifetime. The mean lifetime of the emission at 460 nm was calculated as 3.01 ± 0.085 ns for DqTp and 2.87 ± 0.12 ns for WC@DqTp (see eq S1 for details).[43]

Photoelectrochemical measurements of the photocatalyst immobilized on FTO showed a clear enhancement in photocurrent compared to its bare components, suggesting better charge carrier mobility or a decreased recombination in WC@DqTp (Figure 4f). These data agree well with electrochemical impedance spectroscopy (EIS) results, indicating a higher conductivity in the nanocomposite WC@DqTp in comparison with DqTp and WC (Figure S1c).

Inspired by their promising physicochemical properties, we studied WC@DqTp and its individual components as photocatalysts for hydrogen evolution from water in the absence of an added sacrificial agent. Under simulated solar light, DqTp produced 21.2 ± 4.9 μmol H_2 h^{-1} g_{cat}^{-1} using Pt as a co-catalyst and methyl viologen (MV) as a mediator. In contrast, WC produced no H_2 under identical conditions, likely due to its conduction band minimum located at +0.6 V vs NHE, which is unsuitable for hydrogen evolution. Interestingly, the nanocomposite WC@DqTp showed a photocatalytic H_2 evolution activity of 36.1 ± 5.6 μmol H_2 h^{-1} g_{cat}^{-1}, approximately two times higher than that of DqTp (Figure 5a). The activity was significantly lower at higher pH values (pH 4 and 7) and in the absence of MV, indicating the electron transfer is rate-limiting. In turn, this finding supports our hypothesis of improved electron transfer in the WC@DqTp nanocomposite, leading to improved photocatalytic activity. Control experiments without photocatalyst, co-catalyst, or light produced no H_2 under identical conditions (Figure 5b, see Table S2 for full optimization details). The addition of a sacrificial electron donor led to the suppression of H_2 production, suggesting that water serves as the electron source. However, attempts to detect O_2 formation were not successful due to air leakage during sample preparation affecting the limit of detection. The apparent quantum yield under optimized conditions was determined under AM 1.5G irradiation using the reported protocol, resulting in a value of 0.26%.[44] The chemical and structural stability of WC@DqTp during photocatalysis was confirmed by post-catalysis characterization. FTIR spectra of the used photocatalyst show no change in the chemical structure (Figure S6a). Similarly, the morphology of the used photocatalyst remains intact, according to FESEM analysis (Figure S6b). Table S3 shows that the performance of WC@DqTp compares well with that of other COF-based nanocomposites that have been used as photocatalysts for H_2 generation. WC@DqTp is the only waste-derived porous organic nanocomposite that was successful in the production of green H_2 from water without the addition of a sacrificial agent. Although the activity of WC@DqTp is lower than that of metal-based COF nanocomposites, this photocatalyst represents a sustainable approach toward green hydrogen production through waste-derived photocatalysts and opens up new horizons for future exploration. The ecofriendly and cost-effective nature of WC@DqTp is particularly evident from the increased H_2 production compared to that of pure DqTp, even though WC@DqTp has a lower DqTp content. When normalizing the H_2 production to the amount of nonwaste starting materials consumed during photocatalyst synthesis, WC@DqTp needs only 22.5% of these resources to produce the same amount of H_2. Future work will have to focus on the scale-up of both the synthesis and its application for photocatalytic H_2 production in real-world quantities, for example, in a continuous flow setup. Assessing the stability as well as a full life-cycle assessment will be required to fully appraise the carbon footprint and energy balance of the process.

A proposed photocatalytic mechanism for green H_2 production using WC@DqTp is shown in Figure 6. Upon irradiation of the photocatalyst, both the DqTp and WC constituents undergo photoexcitation. Excited electrons in the DqTp conduction band (CB) will transfer to Pt to evolve H_2, while valence band (VB) holes in the WC can promote water oxidation. From the determined band structure, it can be inferred that excited electrons in the WC CB will transfer to the DqTp VB, thus forming a Z-scheme heterojunction.[45] This mechanism explains the improved photocatalytic activity compared to that of pure DqTp due to the more effective charge separation and a more positive potential of the VB holes having a greater driving force for water oxidation.

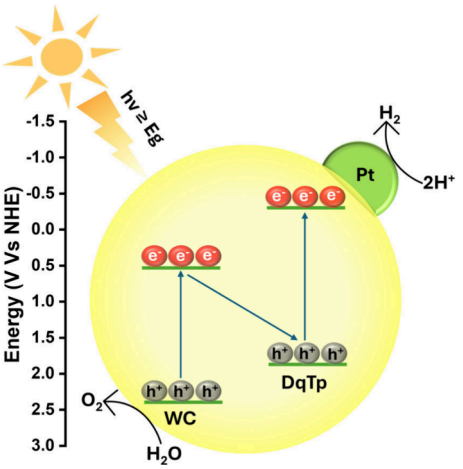

Figure 6. Proposed mechanism for photocatalytic H_2 production using the WC@DqTp photocatalyst.

CONCLUSIONS

In summary, we have demonstrated the one-pot synthesis of a visible-light-active photocatalyst by combining waste coffee (WC) with a porous polymer (DqTp) as an innovative approach to turning waste into valuable products. The resulting visible-light-responsive nanocomposite, WC@DqTp, showed a promising activity of 36.1 ± 5.6 μmol H_2 h^{-1} g_{cat}^{-1} as a photocatalyst for green H_2 production from water, nearly two times more than the H_2 production rate of bare DqTp. In-depth characterization of its optoelectronic properties attributes this performance to enhanced charge separation and transport as a result of the nanocomposite forming a Z-scheme heterojunction between the porous polymer and the coffee waste.

https://doi.org/10.1021/acssusresmgt.5c00454
ACS Sustainable Resour. Manage. 2026, 3, 45−51

■ ASSOCIATED CONTENT

Supporting Information

The Supporting Information is available free of charge at https://pubs.acs.org/doi/10.1021/acssusresmgt.5c00454.

Experimental details; additional catalyst characterization by FTIR, EIS, XPS, UPS, and SEM; optimized parameters for photocatalytic H_2 production; and literature comparison (PDF)

■ AUTHOR INFORMATION

Corresponding Author

Moritz F. Kühnel − *Institute of Chemistry, University of Hohenheim, 70599 Stuttgart, Germany*; Email: moritz.kuehnel@uni-hohenheim.de

Authors

Astha Singh − *Institute of Chemistry, University of Hohenheim, 70599 Stuttgart, Germany*

Swadhin K. Jena − *School of Chemical Sciences, Indian Institute of Technology Mandi, Mandi 175001, India*; orcid.org/0000-0002-1197-5036

Prem F. Siril − *School of Chemical Sciences, Indian Institute of Technology Mandi, Mandi 175001, India*; orcid.org/0000-0002-8818-7310

Complete contact information is available at: https://pubs.acs.org/10.1021/acssusresmgt.5c00454

Author Contributions

Astha Singh: investigation, conceptualization, methodology, experimentation, data curation and analysis, validation, visualization, writing − original draft. Swadhin K. Jena: data curation. Prem F. Siril: review and editing. Moritz F. Kühnel: project administration and discussion, review and editing, funding acquisition.

Notes

The authors declare no competing financial interest.

■ ACKNOWLEDGMENTS

The authors thank the Core Facility at University of Hohenheim for access to their facilities. The authors are also thankful to the Advanced Materials Research Centre (AMRC), IIT Mandi for the electrochemistry experiments, XPS, and FESEM characterization.

■ REFERENCES

(1) Salah, C.; Cobo, S.; Pérez-Ramírez, J.; Guillén-Gosálbez, G. Environmental Sustainability Assessment of Hydrogen from Waste Polymers. *ACS Sustain. Chem. Eng.* **2023**, *11* (8), 3238−3247.

(2) Hossain Bhuiyan, M. M.; Siddique, Z. Hydrogen as an Alternative Fuel: A Comprehensive Review of Challenges and Opportunities in Production, Storage, and Transportation. *Int. J. Hydrog. Energy* **2025**, *102*, 1026−1044.

(3) Bollmann, J.; Pitchaimuthu, S.; Kühnel, M. F. Challenges of Industrial-Scale Testing Infrastructure for Green Hydrogen Technologies. *Energies* **2023**, *16* (8), 3604.

(4) Khandelwal, R. Chapter 3 - Technologies for Water Splitting. *Photochemical Splitting of Water*; George, S. C., Kurian, S., Santos, L. P. M., Eds.; Elsevier, 2025; pp 51−73. DOI: 10.1016/B978-0-443-29064-0.00014-0.

(5) Pinaud, B. A.; Benck, J. D.; Seitz, L. C.; Forman, A. J.; Chen, Z.; Deutsch, T. G.; James, B. D.; Baum, K. N.; Baum, G. N.; Ardo, S.; Wang, H.; Miller, E.; Jaramillo, T. F. Technical and Economic Feasibility of Centralized Facilities for Solar Hydrogen Production via Photocatalysis and Photoelectrochemistry. *Energy Environ. Sci.* **2013**, *6* (7), 1983−2002.

(6) Younas, M.; Shafique, S.; Hafeez, A.; Javed, F.; Rehman, F. An Overview of Hydrogen Production: Current Status, Potential, and Challenges. *Fuel* **2022**, *316*, 123317.

(7) B, A.; A, J.; Rao, A. S.; Nagarkar, S. S.; Dutta, A.; Duttagupta, S. P.; Prabhu, S. S.; Pinto, R. Challenges in Photocatalytic Hydrogen Evolution: Importance of Photocatalysts and Photocatalytic Reactors. *Int. J. Hydrog. Energy* **2024**, *81*, 1442−1466.

(8) Ahmad, I.; AlFaify, S. A.; Alanezi, K. M.; Alfaifi, M. Q.; Abduljawad, M. M.; Liu, Y. Improved Hydrogen Production Performance of an S-Scheme Nb2O5/La2O3 Photocatalyst. *Dalton Trans.* **2025**, *54* (4), 1402−1417.

(9) Ahmad, I.; Shukrullah, S.; Naz, M. Y.; Bhatti, H. N. Dual S-Scheme ZnO-g-C3N4-CuO Heterosystem: A Potential Photocatalyst for H2 Evolution and Wastewater Treatment. *React. Chem. Eng.* **2023**, *8* (5), 1159−1175.

(10) Yang, Q.; Luo, M.; Liu, K.; Cao, H.; Yan, H. Covalent Organic Frameworks for Photocatalytic Applications. *Appl. Catal. B Environ.* **2020**, *276*, 119174.

(11) Teng, J.; Li, W.; Wei, Z.; Hao, D.; Jing, L.; Liu, Y.; Dai, H.; Zhu, Y.; Ma, T.; Deng, J. Coupling Photocatalytic Hydrogen Production with Key Oxidation Reactions. *Angew. Chem. Int. Ed.* **2024**, *63* (50), No. e202416039.

(12) El-Khair, M. A. A.; Al-Gamal, A. G.; Kabel, K. I.; Gado, W. S.; Morshedy, A. S. Harvesting the Synergistic Effect of CuFe2O4@Ni-MOF Nanomagnetic Photocatalyst for Enhanced Visible Light-Driven Green Hydrogen Production. *Int. J. Hydrog. Energy* **2025**, *101*, 280−294.

(13) Ashraf, M.; Ullah, N.; Khan, I.; Tremel, W.; Ahmad, S.; Tahir, M. N. Photoreforming of Waste Polymers for Sustainable Hydrogen Fuel and Chemicals Feedstock: Waste to Energy. *Chem. Rev.* **2023**, *123* (8), 4443−4509.

(14) Jones, B.; Davies, K. R.; Allan, M. G.; Anantharaj, S.; Mabbett, I.; Watson, T.; Durrant, J. R.; Kuehnel, M. F.; Pitchaimuthu, S. Photoelectrochemical Concurrent Hydrogen Generation and Heavy Metal Recovery from Polluted Acidic Mine Water. *Sustain. Energy Fuels* **2021**, *5* (12), 3084−3091.

(15) Uekert, T.; Kuehnel, M. F.; Wakerley, D. W.; Reisner, E. Plastic Waste as a Feedstock for Solar-Driven H2 Generation. *Energy Environ. Sci.* **2018**, *11* (10), 2853−2857.

(16) Bashir, I.; McGettrick, J. D.; Kühnel, M. F.; Sarfraz, B.; Arshad, S. N.; Rauf, A. Sustainable Formate Synthesis: Integrating Ethylene Glycol Oxidation with Carbon Dioxide Electrocatalysis Using Redox-Stabilized Earth-Abundant Electrodes. *ACS Sustain. Chem. Eng.* **2024**, *12* (12), 4795−4802.

(17) Boukayouht, K.; Bazzi, L.; El Hankari, S. Sustainable Synthesis of Metal-Organic Frameworks and Their Derived Materials from Organic and Inorganic Wastes. *Coord. Chem. Rev.* **2023**, *478*, 214986.

(18) Cao, K.; Zhang, S.; Shi, Y.; Diao, X.; Wei, R.; Ji, N. Catalytic Upgrading of Plastic Wastes into High-Value Carbon Nanomaterials: Synthesis and Applications. *ACS Nano* **2025**, *19* (13), 12734−12761.

(19) Ma, Q.; Yu, Y.; Sindoro, M.; Fane, A. G.; Wang, R.; Zhang, H. Carbon-Based Functional Materials Derived from Waste for Water Remediation and Energy Storage. *Adv. Mater.* **2017**, *29* (13), 1605361.

(20) Priya, A. K.; Muruganandam, M.; Suresh, S. Bio-Derived Carbon-Based Materials for Sustainable Environmental Remediation and Wastewater Treatment. *Chemosphere* **2024**, *362*, 142731.

(21) Kharangarh, P. R.; Ravindra, N. M.; Singh, G.; Umapathy, S. Synthesis of Luminescent Graphene Quantum Dots from Biomass Waste Materials for Energy-Related Applications—An Overview. *Energy Storage* **2023**, *5* (3), No. e390.

(22) Xue, B.; Xu, J.; Xiao, R. Synthesis of Hierarchically Porous Carbon with Tailored Porosity and Electrical Conductivity Derived from Hard-Soft Carbon Precursors for Enhanced Capacitive Performance. *ACS Sustain. Chem. Eng.* **2021**, *9* (47), 15925−15934.

(23) Demarema, S.; Nasr, M.; Ookawara, S.; Abdelhaleem, A. New Insights into Green Synthesis of Metal Oxide Based Photocatalysts for

Photodegradation of Organic Pollutants: A Bibliometric Analysis and Techno-Economic Evaluation. *J. Clean. Prod.* **2024**, *463*, 142679.
(24) ICO. *Annual Review Coffee Year 2021/2022*; International Coffee Organization (ICO), London, UK, 2022.
(25) Cervera-Mata, A.; Delgado, G.; Fernández-Arteaga, A.; Fornasier, F.; Mondini, C. Spent Coffee Grounds By-Products and Their Influence on Soil C-N Dynamics. *J. Environ. Manage.* **2022**, *302*, 114075.
(26) Pongsiriyakul, K.; Wongsurakul, P.; Kiatkittipong, W.; Premashthira, A.; Kuldilok, K.; Najdanovic-Visak, V.; Adhikari, S.; Cognet, P.; Kida, T.; Assabumrungrat, S. Upcycling Coffee Waste: Key Industrial Activities for Advancing Circular Economy and Overcoming Commercialization Challenges. *Processes* **2024**, *12* (12), 2851.
(27) Tsigkou, K.; Demissie, B. A.; Hashim, S.; Ghofrani-Isfahani, P.; Thomas, R.; Mapinga, K. F.; Kassahun, S. K.; Angelidaki, I. Coffee Processing Waste: Unlocking Opportunities for Sustainable Development. *Renew. Sustain. Energy Rev.* **2025**, *210*, 115263.
(28) Singh, A.; Gogoi, R.; Sharma, K.; Fourati, N.; Zerrouki, C.; Remita, S.; Felix Siril, P. Continuous Flow Synthesis of Ag-PEDOT-COF Nanocomposite for Sustainable Photoreforming of Plastic Waste and Chromium Remediation in Visible Light. *Sep. Purif. Technol.* **2023**, *323*, 124459.
(29) Li, Q.; Lan, X.; An, G.; Ricardez-Sandoval, L.; Wang, Z.; Bai, G. Visible-Light-Responsive Anthraquinone Functionalized Covalent Organic Frameworks for Metal-Free Selective Oxidation of Sulfides: Effects of Morphology and Structure. *ACS Catal.* **2020**, *10* (12), 6664−6675.
(30) Ballesteros, L. F.; Teixeira, J. A.; Mussatto, S. I. Chemical, Functional, and Structural Properties of Spent Coffee Grounds and Coffee Silverskin. *Food Bioprocess Technol.* **2014**, *7* (12), 3493−3503.
(31) Kabayo, S. M.; Kindala, J. T.; Nkanga, C. I.; Krause, R. W. M.; Taba, K. M. Preparation and Characterization of Solid Acid Catalysts Derived from Coffee Husks. *Int. J. Chem. Sci.* **2019**, *3* (6), 5−13.
(32) Mei, D.; Yan, B. Defect Engineering in β-Ketoenamine-Linked Covalent Organic Frameworks for High-Efficiency Uranium Extraction. *J. Mater. Chem. A* **2025**, *13*, 14928.
(33) Kong, X.; Zhou, S.; Strømme, M.; Xu, C. Redox Active Covalent Organic Framework-Based Conductive Nanofibers for Flexible Energy Storage Device. *Carbon* **2021**, *171*, 248−256.
(34) Ellerbrock, R. H.; Gerke, H. H. FTIR Spectral Band Shifts Explained by OM-Cation Interactions. *J. Plant Nutr. Soil Sci.* **2021**, *184* (3), 388−397.
(35) Singh, A.; Gogoi, R.; Sharma, K.; Jena, S. K.; Fourati, N.; Zerrouki, C.; Remita, S.; Siril, P. F. Continuous Flow Synthesis of Visible Light-Active Conjugated Porous Polymer for Pollutant Degradation and Plastic Waste Photoreforming. *J. Clean. Prod.* **2023**, *428*, 139476.
(36) Guo, S.; Yang, P.; Zhao, Y.; Yu, X.; Wu, Y.; Zhang, H.; Yu, B.; Han, B.; George, M. W.; Liu, Z. Direct Z-Scheme Heterojunction of SnS_2 /Sulfur-Bridged Covalent Triazine Frameworks for Visible-Light-Driven CO_2 Photoreduction. *ChemSusChem* **2020**, *13* (23), 6278−6283.
(37) Singh, A.; Gogoi, R.; Sharma, K.; Kumar, R.; Siril, P. F. Continuous Flow Synthesis of Disordered Covalent Organic Framework for Ultra-High Removal of Industrial Pollutants in Flow. *Sep. Purif. Technol.* **2023**, *307*, 122739.
(38) Cychosz, K. A.; Guillet-Nicolas, R.; García-Martínez, J.; Thommes, M. Recent Advances in the Textural Characterization of Hierarchically Structured Nanoporous Materials. *Chem. Soc. Rev.* **2017**, *46* (2), 389−414.
(39) Dautzenberg, E.; Lam, M.; Nikolaeva, T.; Franssen, W. M. J.; van Lagen, B.; Gerrits-Benneheij, I. P. A. M.; Kosinov, N.; Li, G.; de Smet, L. C. P. M. Tuning UV Absorption in Imine-Linked Covalent Organic Frameworks via Methylation. *J. Phys. Chem. C* **2022**, *126* (50), 21338−21347.
(40) Gogoi, R.; Singh, A.; Moutam, V.; Sharma, L.; Sharma, K.; Halder, A.; Siril, P. F. Revealing the Unexplored Effect of Residual Iron Oxide on the Photoreforming Activities of Polypyrrole Nanostructures on Plastic Waste and Photocatalytic Pollutant Degradation. *J. Environ. Chem. Eng.* **2022**, *10* (2), 106649.
(41) Wang, Z.; Yeary, P.; Fan, Y.; Lin, W. Anthraquinone-Based Covalent Organic Framework as a Recyclable Direct Hydrogen Atom Transfer Photocatalyst for C-H Functionalization. *Chem. Sci.* **2024**, *15* (13), 4920−4925.
(42) Jiang, L.; Yuan, X.; Zeng, G.; Wu, Z.; Liang, J.; Chen, X.; Leng, L.; Wang, H.; Wang, H. Metal-Free Efficient Photocatalyst for Stable Visible-Light Photocatalytic Degradation of Refractory Pollutant. *Appl. Catal. B Environ.* **2018**, *221*, 715−725.
(43) Li, Q.; Lan, X.; An, G.; Ricardez-Sandoval, L.; Wang, Z.; Bai, G. Visible-Light-Responsive Anthraquinone Functionalized Covalent Organic Frameworks for Metal-Free Selective Oxidation of Sulfides: Effects of Morphology and Structure. *ACS Catal.* **2020**, *10* (12), 6664−6675.
(44) Abd El Salam, H. M.; Morshedy, A. S. TiO2@Metal Organic Framework Ni2(BDC)2(DABCO) as an Efficient Water Splitting Heterogeneous Photocatalyst for Enhanced Green Hydrogen Generation under Visible Light. *Int. J. Hydrog. Energy* **2025**, *151*, 150142.
(45) El Sharkawy, H. M.; Abo El-Khair, M. A.; Morshedy, A. S. Construction of SnS2@SnO2 nanocomposite Z-scheme heterojunction for dual-functional photocatalysis: Green hydrogen generation and crystal violet degradation. *Int. J. Hydrog. Energy* **2025**, *137*, 471−486.

https://doi.org/10.1021/acssusresmgt.5c00454
ACS Sustainable Resour. Manage. 2026, 3, 45−51